TECHNICAL UNIVERSITY OF CLUJ-NAPOCA

ACTA TECHNICA NAPOCENSIS

Series: Applied Mathematics, Mechanics, and Engineering
Vol. 65, Issue IV, November, 2022

EVALUATION OF THE POTENTIAL DEFORMATION ENERGY FROM THE ELASTIC ELEMENT OF A BIONIC DISPLACEMENT SYSTEM

Adrian - Ioan BOTEAN

Abstract: *In this paper, I present a multidisciplinary approach to establishing the maximum loaded cross-section of the elastic element of the bionic displacement system (whose conception must base on the principle of biomimicry), as well as the evaluation of the state of stresses and strains respectively of the accumulated potential deformation energy. This study involves modeling the structure using the finite element method for efforts evaluation (axial force N, shear force T, and bending moment Mi), the use of analytical models for calculating mechanical stresses and potential deformation energy, and the use of electrical strain-gages method to experimental evaluation of strains. The evaluation of strains (a total of 2,979 processed data) is performed in two working scenarios: for the case where there is bipedal support (S1) and for the case of unipedal support, for uniform rectilinear movement (S2). In both scenarios, the relative deviations (concerning the potential deformation energy) between the analytically and experimentally obtained results are below 11 percent. This study has relevance, especially from the perspective of the possibility of optimally dimensioning the elastic element so that the bionic displacement system has its mass as small as possible.*

Keywords: *potential deformation energy, bionic displacement system, reactions, internal forces, finite element method, mechanical stresses, strain, strain gauges*

1. INTRODUCTION

Potential deformation energy or elastic energy is the energy stored in a mechanically stressed body in the field of elastic deformations. Nature is an inexhaustible source of ideas applicable in various branches of technology and has allowed the development of new technologies, and the creation of structures, materials, or devices.

One of the aspects studied from the point of view of bionics and which led to the finding of many solutions, both technical and medical, is the human and animal movement [1-4]. There are a variety of biological entities that move in different forms, depending on the structure of the body or limbs [5-7]. For example, fleas can jump up to 18 cm vertically and 33 cm horizontally, being among the best jumpers among animals in terms of weight. This fast and energetic movement of the hind legs is achieved using an elastic protein called resilin, which before the jump can be tensed like a spring, thus storing potential deformation energy [8]. A large animal that jumps as a mode of locomotion is the kangaroo. It weighs about 90 kg and can reach 1.8 m when standing upright. Kangaroos use the potential deformation energy at each jump, thus lowering the strain on the muscles and causing more efficient oxygen burning than in other mammals of similar size. The key element in the movement of the kangaroo is the tendon in the lower limbs, which is the structure through which the force of the muscles is transmitted to the skeleton [9 - 12].

The paper entitled "Evaluation of the potential deformation energy of the elastic element of a bionic displacement system" is an approach to establishing the maximum loaded cross-section of the elastic element of the bionic displacement system, represented in Figure 1 [13], (whose conception must base on the principle of biomimicry) as well as the evaluation of the state of stresses and deformations respectively of the accumulated potential deformation energy.

Received: 06.09.22; **Similarities**: 19.10.22: **Reviewed**: 05.11./01.11.22: **Accepted**:17.11.22.

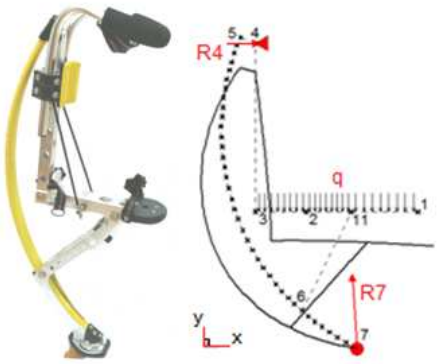

Fig. 1. Bionic displacement system: left - real model, right – in plane modeling, performed in the finite element analysis program RDM 6.19 [13].

The elastic element is made of a homogeneous and anisotropic composite material (glass E - 73.3% by volume - in epoxy - parallel load with continuous fibers - for which the longitudinal modulus of elasticity or Young's modulus is E = 0.56E5 MPa, the transverse contraction coefficient or Poisson's ratio $\mu = 0.26$ [14, 15] and the breaking limit (ultimate stress) $\sigma_r = 500$ MPa [16, 17]) for which the anisotropic linear-elastic model is applied, where Robert Hooke's law represents a simplifying hypothesis [18, 19].

This study involves modeling the structure using the finite element method for internal forces evaluation (axial force N, shear force T, and bending moment Mi), the use of analytical models for calculating mechanical stresses and potential deformation energy, and the use of the electrical strain-gages method to experimental evaluation.

The external forces applied to the bionic displacement system are in static equilibrium (q = 2,616 N/mm - unipedal position), R4 = 52.1 N, R7 having the components Rx = 52.1 N and Ry = 781.6 N) and the internal loads (normal force N, the shear force T and the bending moment Mi) are distributed according to Figure 2 (Nmax = N_{max} = 589.54 N, Tymax = T_{max} = 666.41 N, Mzmax = Mi_{max} = 85,308.24 N·mm) [13]. Qualitative and quantitative evaluation of the reaction vectors as well as of the internal forces was performed through the finite element analysis program RDM 7.04 [13].

The elastic element (as a component element of the bionic displacement system) represents a curved bar which, as in the case of straight bars loaded for bending, is the maximum stress in the section where the bending moment (in this case Mz) has a maximum value. Thus, the maximum bending moment is recorded at an angle of 37 degrees concerning the bounded segment using nodes 6 - 11. In this cross-section the axial force N = -467.1 N, the shear force T = -7.3 N and the Mimax = 85,308.24 N·mm. The semicircular elastic element has a variable cross-section, according to Figure 3, presenting a complex geometry for which the characteristic dimensions are highlighted in Figure 4.

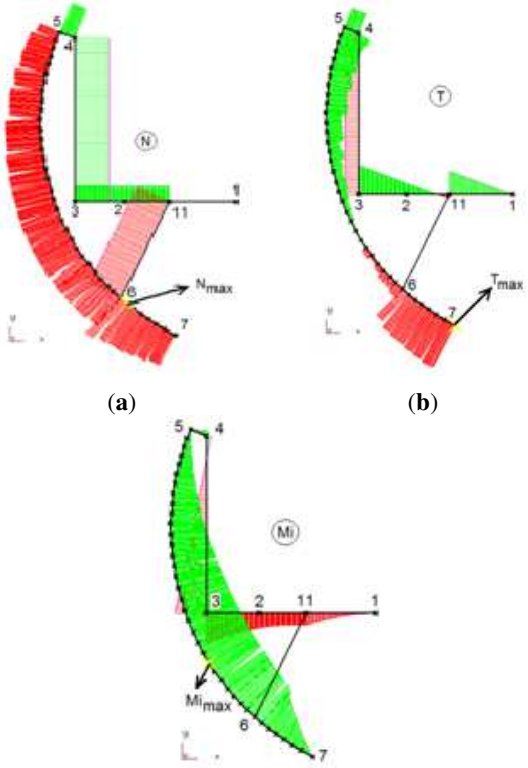

(**a**) (**b**)

(**c**)

Fig. 2. Variation diagrams of efforts in the bionic displacement system [13]. (**a**) normal force (N); (**b**) shear force (T); (**c**) bending moment (Mi).

Fig. 3. Highlighting the variable cross-section of the elastic element.

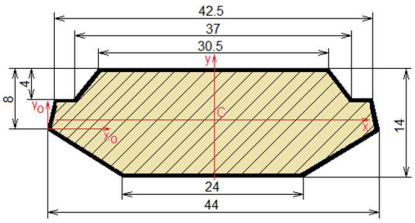

Fig. 4. Cross-section with the complex geometry of the semicircular element.

For the cross-section with the complex geometry of the semicircular element, defined in Figure 4, the geometric characteristics are the following:

-the perimeter of the considered surface: p = 101.77 mm;

-the area of the considered surface: A = 512 mm;

-position of the center of gravity in relation to the xy reference axis system expressed by the relations:

$$x_C = \frac{\sum_{i=1}^{n} x_i \cdot A_i}{\sum_{i=1}^{n} A_i} \quad (1)$$

$$y_C = \frac{\sum_{i=1}^{n} y_i \cdot A_i}{\sum_{i=1}^{n} A_i} \quad (2)$$

x_c=22 mm, y_c=1.1589 mm;

-central or equatorial moments of inertia (defined by the Steiner - Huygens relations):

$$I_x = \sum_{i=1}^{n} (I_{xi} + y_{ci} \cdot A_i) \quad (3)$$

$$I_y = \sum_{i=1}^{n} (I_{yi} + x_{ci} \cdot A_i) \quad (4)$$

$$I_{xy} = \sum_{i=1}^{n} (I_{x_i y_i} + x_{ci} \cdot y_{ci} \cdot A_i) \quad (5)$$

I_x=7,251.08 mm^4, I_y=61,260.67 mm^4, I_{xy}=0. The centrifugal moment of inertia I_{xy} is zero because the y-axis is the axis of symmetry for the considered surface. Thus, the main directions coincide with the central reference axes.

-section modules in relation to the central reference axes:

$$W_x = \frac{I_x}{y_{max}} \quad (6)$$

$$W_y = \frac{I_y}{x_{max}} \quad (7)$$

W_x=1,012.88 mm^3, W_y=2,784.58 mm^3;

-the static moments of the two sections concerning the central axis x:

For the section below the x-axis:

$$S_x = A_i \cdot y_i \quad (8)$$

where A_i is the area of the cross-sectional area located at the bottom of the central axis x and y_i represents the distance from the center of gravity of this surface to the central axis x.

A_i=254.74 mm^2, y_i=3.2106 mm, S_x=817.868 mm^3;

For the section above the x-axis:

$$S_x = A_s \cdot y_s \quad (9)$$

where A_s is the area of the cross-sectional area located at the top of the central axis x and y_s represent the distance from the center of gravity of this surface to the central axis x.

A_s=257.26 mm^2, y_s=3.179 mm, S_x=817.829 mm^3.

In the case of curved bars, the state of stresses (with reference here to normal stresses σ) is determined using Winkler's formula which can be expressed for the following two distinct situations:

a) if it is considered that the bending moment has a maximum influence (simple bending load) Winkler's formula is as follows:

$$\sigma = \frac{M_i}{e \cdot A} \cdot \frac{y}{r - y} \quad (10)$$

To explain the terms in relation (10), approximate the cross section with a rectangle, according to Figure 5.

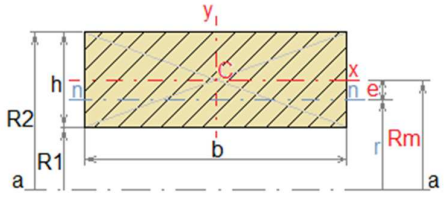

Fig. 5. The cross-section with complex geometry is approximated as a rectangle to explain Winkler's formula.

From Figure 5 the following terms can be highlighted:

- a-a is the axis of curvature of the semicircular bar;

-R1 is the inner radius of the semicircular bar;

-R2 represents the outer radius of the semicircular bar;

-Rm is the mean radius expressed by the following relation (Rm = 556 mm):

$$Rm = \frac{R1 + R2}{2} \quad (11)$$

- n-n represents the neutral axis (layer or fiber of material in which the normal stress σ is zero - in case of simple bending load the neutral axis coincides with the central axis x);

- r is the radius of curvature of the neutral axis, for the rectangular section expressed by the following relation:

$$r = \frac{h}{ln\frac{R2}{R1}} \cong \frac{Rm}{1 + \frac{1}{3} \cdot \left(\frac{h}{2 \cdot Rm}\right)^2} \quad (12)$$

- e represents the distance from the neutral axis n -n to the central axis x and can be determined with the help of the following relation:

$$e = Rm - r \cong \frac{h^2}{12 \cdot Rm} \quad (13)$$

- dimension y specifies the position of the material fiber about the central axis x in which the evaluation of the normal stress σ is pursued.
b) if we consider the influence of normal effort N, Winkler's formula is:

$$\sigma = \frac{N}{A} + \frac{M_i}{e \cdot A} \cdot \frac{y}{r - y} \quad (14)$$

Since the ratio between the mean radius Rm and the total height of section is greater than 10, the circular bar is considered to have a large radius of curvature in which case the normal stress σ can be determined with satisfactory results by Navier's formula, as follows [16, 20-22]:

$$\sigma = \frac{Mi}{W_x} = \frac{Mi}{I_x} \cdot y \quad (15)$$

If we consider, the effect of the axial force N (we will speak here of compound stress of type σ + σ) the relation (15) will be of the form:

$$\sigma = \frac{N}{A} + \frac{Mi}{W_x} = \frac{N}{A} + \frac{Mi}{I_x} \cdot y \quad (16)$$

In this case the position of the neutral axis is:

$$e = y = -\frac{N}{Mi} \cdot \frac{I_x}{A} \quad (17)$$

The shear stress T generates in the same cross-section the tangential stress τ which can be evaluated using of the Juravschi relation, having the following form:

$$\tau = \frac{T \cdot S_x}{b \cdot I_x} \quad (18)$$

where b represents the width of the cross-section corresponding to the center of gravity.

The relation (18) can be customized for the geometry of the cross-section of the semicircular bar considered in this study as follows (according to Figure 6).

$$S_x = \int_y^{\frac{h}{2}} y \cdot dA = \int_y^{\frac{h}{2}} y \cdot b \cdot dy = \\ = \frac{b}{2} \cdot \left(\frac{h^2}{4} - y^2\right) \quad (19)$$

$$I_x = \frac{b \cdot h^3}{12} \quad (20)$$

By replacing relations (19) and (20) in relation (18) it results:

$$\tau = \frac{6 \cdot T}{b \cdot h^3} \cdot \left(\frac{h^2}{4} - y^2\right) \quad (21)$$

The tangential stresses τ produce a longitudinal slip effect of the material layers, especially those near the center of gravity of the cross-section.

From the analysis of the relations that express the variation of the normal stress σ and the shear stress τ it can be noticed that the normal stresses have maximum values at the level of extreme material fibers (inner fiber and outer fiber) and the shear stresses are maximum in the center of gravity of the cross-section, according to Figure 7.

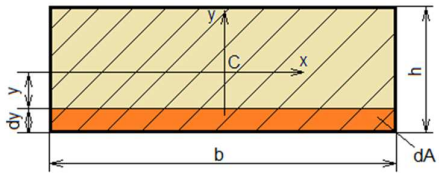

Fig. 6. Customization of Juravschi's formula for the rectangular cross section.

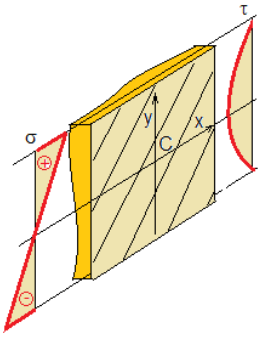

Fig. 7. Distribution of normal σ and shear stresses τ in the cross-section of the semicircular elastic element.

The potential deformation energy that is stored in the composite material of the elastic element, because of the elastic deformation produced by the action of external loads, can also be expressed mathematically using normal stresses σ and shear stresses τ.

Thus, the normal stress σ produced by the axial force N generates potential deformation energy expressed by the relation:

$$U_{d1} = \int_V \frac{\sigma^2}{2 \cdot E} \cdot dV = \frac{1}{2} \cdot \sigma \cdot \varepsilon \quad (22)$$

At the bending load, where the shear force T produces the shear stress τ and the bending moment Mi produces the normal stress σ, the potential deformation energy is expressed by the relation:

$$U_{d2} = \int_V \frac{\tau^2}{2 \cdot G} \cdot dV + \int_V \frac{\sigma^2}{2 \cdot E} \cdot dV = \\ = \frac{1}{2} \cdot \tau \cdot \gamma + \frac{1}{2} \cdot \sigma \cdot \varepsilon \qquad (23)$$

where: ε represents the specific linear deformation (strain), γ is the specific slip (angular strain) and G represents the transverse modulus of elasticity.

The transverse modulus of elasticity G can be expressed by means of the longitudinal modulus of elasticity (Young's modulus) E as follows:

$$G = \frac{E}{2 \cdot (1 + \mu)} \qquad (24)$$

Considering that at the same time, for the entire duration of the load, there is a compound load (axial stress in tandem with the simple bending stress) the potential total deformation energy is:

$$U_d = U_{d1} + U_{d2} \qquad (25)$$

The specific linear deformation ε is a parameter that can be evaluated experimentally through various investigation methods: digital image correlation method, interferometric methods, electrical strain-gages method, etc.

With this consideration as a starting point, the method of electrical strain-gages method will be applied in the future for the experimental evaluation of the potential deformation energy.

2. MATERIALS AND METHODS

To establish the optimal mounting variant of strain gauges (TTR) in the Wheatstone resistance bridge (according to Figure 8) the four curves of variation of the output voltage Vo are analyzed comparatively depending on the modification of the resistance/resistances that configure the Wheatstone bridge (Figure 9) [21-30].

Thus, Curve 1 shows the variation of the output voltage V_o depending on the variation of the electrical resistance R1 (Figure 9). The law of variation is not linear, giving satisfactory results for small changes in electrical resistance.

Curve 2 highlights the variation of the output voltage V_o as a function of the change of the opposite resistors R1 and R4 (Figure 9) with the same value. And in this case, the voltage variation diagram is nonlinear, the output voltage Vo being twice higher than in the previous case.

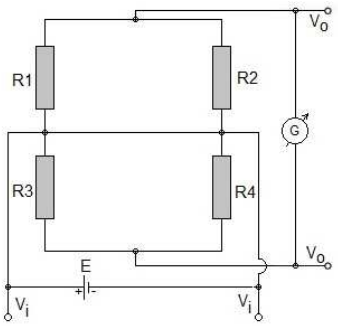

Fig. 8. Wheatstone bridge.

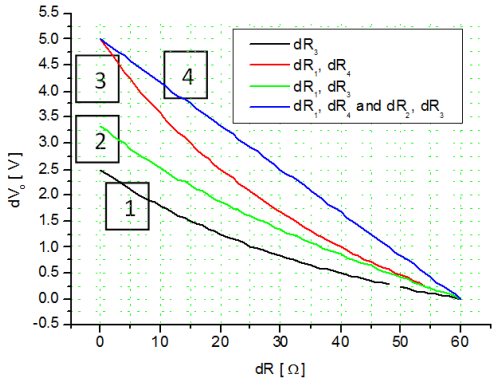

Fig. 9. Modification of the Vo output voltage from the Wheatstone bridge and depending on the variation of the electrical resistance.

Curve 3 represents the variation of the output voltage V_o as a function of the inverse change of the adjacent resistors R1 and R3 (Figure 9). In this case, the diagram looks closer to the linear function.

Curve 4 expresses the variation of the output voltage V_o as a function of the modification of the four electrical resistances that make up the Wheatstone bridge (Figure 9). Thus, the two opposite sets of electrical resistors (R1 R4 and R2 R3) change their value in inverse form. In this case, the shape of the variation curve is approximately linear.

In a median approach, the semi-bridge (half-bridge) mounting (mounting characteristic of curves 2 and 3 in Figure 9) is chosen, considering that the TTR mounting in the semi-bridge can be done adjacent (R1R2 or R3R4) - Figure 10 - or in opposition (R1R3 or R2R4) according to Figure 12.

In the case of half-bridge mounting of adjacent TTRs, their mounting by soldering (according to Figure 10 and Figure 11) is done so that one transducer will measure the strain extension ε (+) and the other transducer will measure the strain compression ε (-).

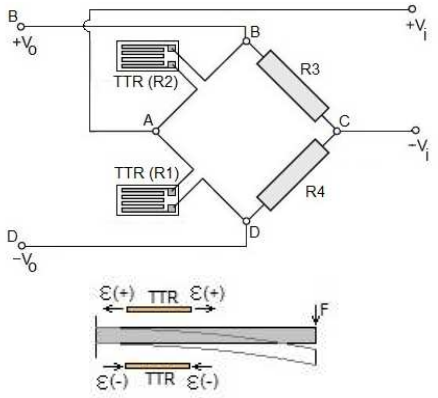

Fig. 10. TTR mounted in the half-bridge, adjacent.

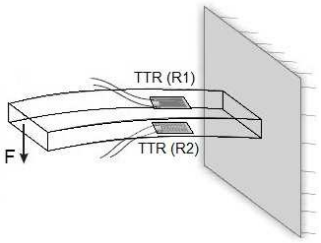

Fig. 11. TTR mounted in the half bridge, adjacent.

Thus, from the relation

$$V_o = \frac{V_i \cdot k \cdot \varepsilon}{4} \qquad (26)$$

result:

$$V_o = \frac{V_i}{4} \cdot k \cdot (\varepsilon_1 - \varepsilon_2) \qquad (27)$$

where:

- k represents the constant of the TTR. For each batch of transducers, the value of this constant is determined experimentally. In general, for the usual TTRs, the constant of the transducer varies in a range of values between 1.9 and 2.3.
- V_i is the input voltage and V_o is the output voltage of the circuit that forms the Wheatstone resistor bridge.

Because

$$\varepsilon_1 = -\varepsilon_2 = \varepsilon$$

the relation (27) becomes:

$$V_o = \frac{V_i}{4} \cdot k \cdot 2 \cdot \varepsilon = \frac{V_i}{2} \cdot k \cdot \varepsilon \qquad (28)$$

The relation (28) represents the calculation relation of the output voltage from the Wheatstone bridge as a function of the modification of the specific linear deformation ε recorded by TTR for the installation in semi-bridge.

In the case of adjacent semi-bridge mounting of TTR, for k = 2 and ε = 1,000 μm/m, according to relation (28), the sensitivity of the circuit will be:

$$\frac{V_o}{V_i} = \frac{k \cdot \varepsilon}{2} = \frac{2 \cdot 1.000 \cdot 10^{-6}}{2} = 1 \frac{mV}{V}$$

In the case of semi-bridge mounting of TTR, in opposition, their gluing (according to Figure 12 and Figure 13) is done so that both transducers will measure the specific linear deformation ε (+) or the specific linear compression deformation ε (-).

Thus, from relation (26) it results:

$$V_o = \frac{V_i}{4} \cdot k \cdot (\varepsilon_1 + \varepsilon_3) \qquad (29)$$

Because

$$\varepsilon_1 = \varepsilon_3 = \varepsilon$$

the relation (29) becomes:

$$V_o = \frac{V_i}{4} \cdot k \cdot 2 \cdot \varepsilon = \frac{V_i}{2} \cdot k \cdot \varepsilon \qquad (30)$$

Relation (30), identical to relation (28), represents the calculation relation of the output voltage from the Wheatstone bridge depending on the modification of the specific linear deformation ε recorded by TTR for the installation in the half-bridge.

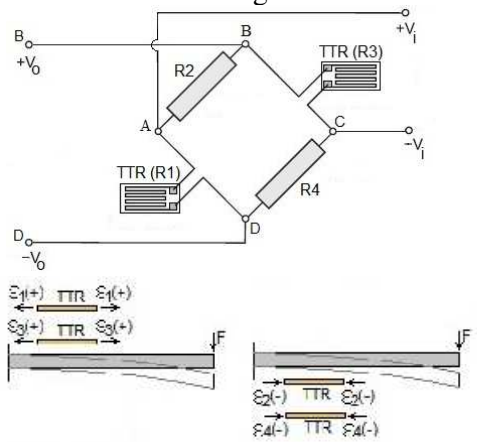

Fig. 12. Half-bridge TTR mounting, opposite.

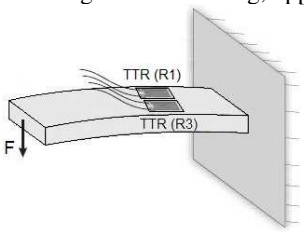

Fig. 13. Half-bridge TTR mounting, opposite.

R. Hooke's law allows the evaluation of the normal stress σ as a function of the longitudinal modulus of elasticity (Young's modulus) E and the specific linear deformation ε according to the relation:

$$\sigma = E \cdot \varepsilon \qquad (31)$$

In this experiment, I chose to mount the TTRs in the half-adjacent bridge (Figure 14) and the TTRs used are type EA-06-250BG-120 produced by Measurement Group, INC., Micro-Measurements Division, with electrical resistance R = 120.0 ± 0.15% Ω and the constant of the transducer is k = 2.075 ± 0.5%.

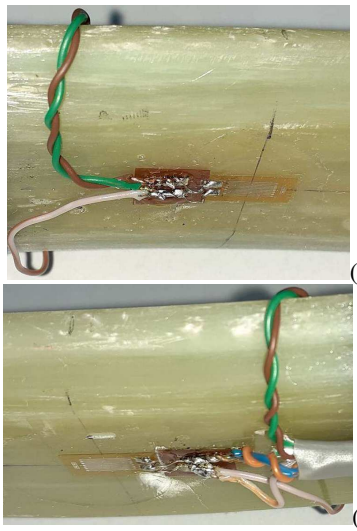

(**a**)

(**b**)

Fig. 14. TTR mounted in the half-bridge, adjacent. (**a**) inner fiber; (**b**) outer fiber.

The Spider 8-30 data acquisition system is used, and its configuration was done using the CatmanEasy V3.3.5 interface, according to Figure 15 and Figure 16, specifying that the Sample rate group selects a frequency of 25 Hz and Automatic zero balancing.

Fig. 15. The experimental stand.

To perform the experimental tests, two types of tests were performed for which the following work scenarios were defined:

S1 - From the sitting position (Figure 17a) we move to bipedal support (Figure 17b) followed by the return to the initial position (Figure 17c);

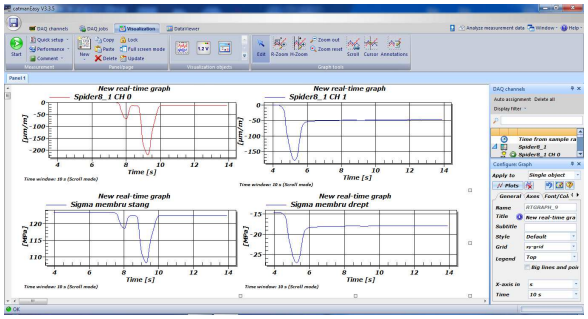

Fig. 16. CatmanEasy V3.3.5 software interface.

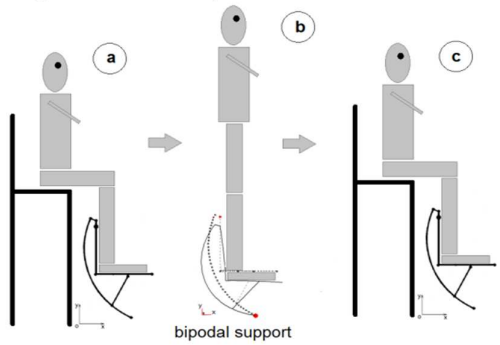

Fig. 17. Graphic representation of the working scenario S1.

S2 - From the bipedal support position (Figure 18a) a uniform rectilinear movement is performed (Figure 18b and Figure 18c) which involves the realization of an alternative unipedal support both at the level of the left lower limb (LF) and at the level of the right lower limb (RF), after which it passes to a final position corresponding to the bipedal support (Figure 18d).

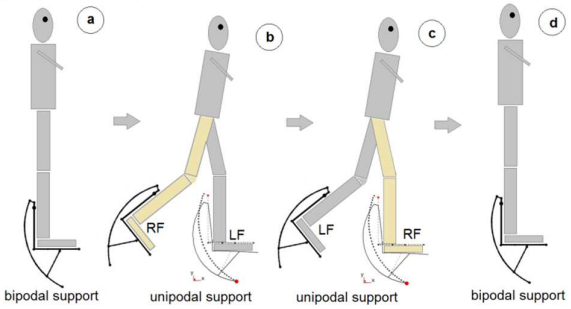

Fig. 18. Graphic representation of the working scenario S2.

For each type of test (S1 and S2) three sets of measurements were performed (Set1, Set2, and Set3), thus obtaining three sets of data. In the case of bipedal support (S1) 467, 429, and 409

data were obtained, resulting in several 1,305 data. For the case of bipedal displacement (S2) 546, 643, and 494 data were obtained, resulting in several 1,674 data. The cumulation of data results in a total of 2,979 processed data. All these data allow, in the next paragraph, to plot the variation diagrams of the specific linear deformation ε as a function of time for the two proposed working scenarios.

3. RESULTS

In the case of the first working scenario (S1), the sitting position is switched to bipedal support followed by the return to the initial position. Thus, Figure 19 shows the variation diagrams of the specific linear deformation (ε) as a function of time for the three data sets recorded by the strain gauges mounted on the bionic displacement system that equips the lower left limb (LF). Generation of these diagrams was possible with the help of the Origin v6.0 program. The mean linear specific strain is plotted (blue line) using the Average Multiple Curves function (from the Analysis module).

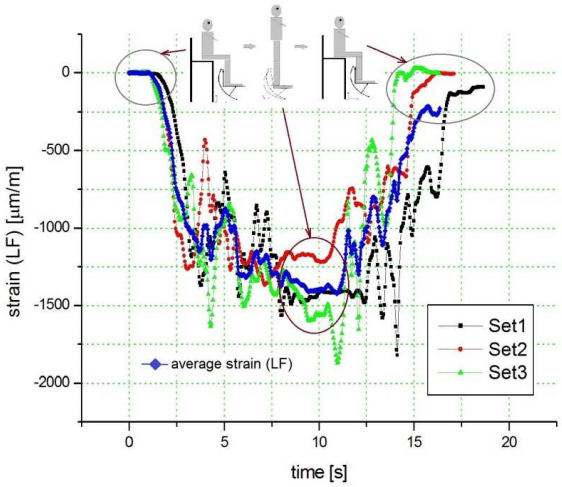

Fig. 19. Variation of linear specific deformation (ε) as a function of time, working scenario 1, left limb (LF).

Figure 20 shows the variation diagrams of the specific linear deformation (ε) as a function of time for the three data sets recorded by the strain gauges mounted on the bionic displacement system that equips the right lower limb (RF). Also, the variation diagram of the specific linear average specific deformation (blue line) is drawn.

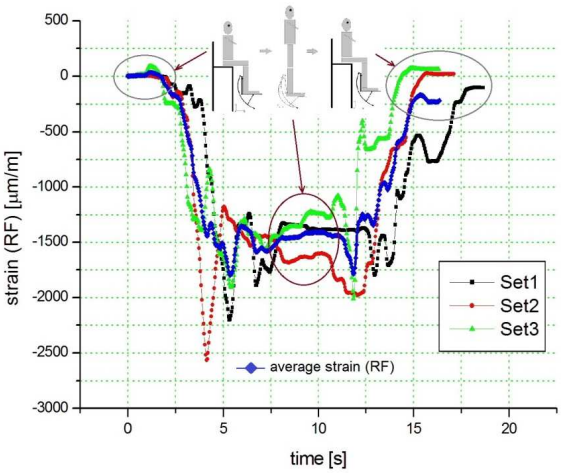

Fig. 20. Variation of linear specific deformation (ε) as a function of time, working scenario 1, right limb (RF).

Figure 21 shows the variation diagrams of the average linear specific deformations (highlighted in Figures 19 and 20) as a function of time. This graphical representation highlights the fact that the static equilibrium position, corresponding to the bipedal support, is reached, now when the two diagrams reach a point of convergence on an approximately constant level. The convergence zone, as shown in Figure 21, is marked by the circular surface A, for which the specific linear deformation has the value ε_{med} = 1,421.7 µm/m.

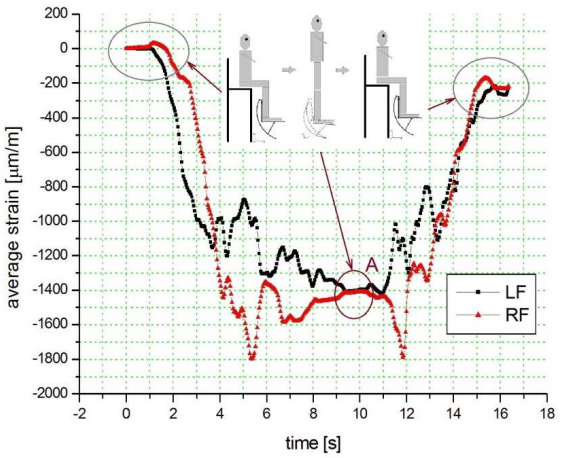

Fig. 21. Variation of mean linear specific deformation (ε_{med}) as a function of time, working scenario 1, left limb (LF), and right limb (RF).

In the second working scenario (S2) when from the bipedal support position, a uniform rectilinear movement is performed which implies the realization of an alternative unipedal support both at the level of the left lower limb (LF) and at the level of the right lower limb (RF),

after which it passes to a final position corresponding to the bipedal support. Figure 22 shows this working scenario for the first data set, drawing the variation diagrams of the specific linear deformation ε as a function of time.

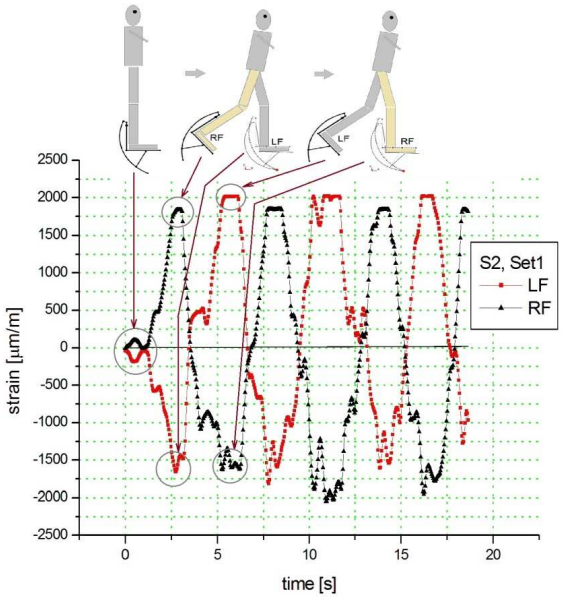

Fig. 22. Variation of specific linear deformation (ε) as a function of time, working scenario 2, for data set 1.

Figure 23 shows the variation diagrams of the specific linear deformation (ε) as a function of time for the three data sets recorded by the strain gauges mounted on the bionic displacement system that equips the left lower limb (LF). The variation diagram of the specific linear average deformation (olive line) is also drawn.

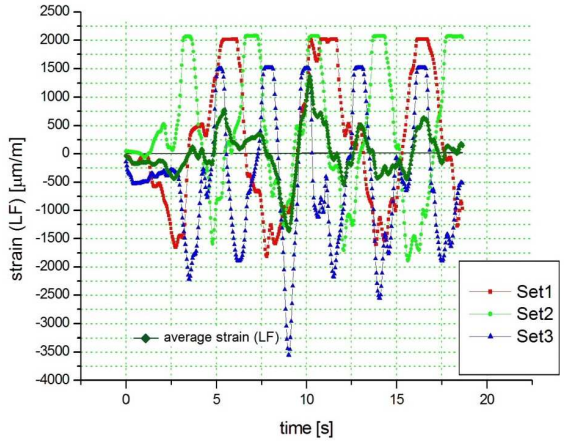

Fig. 23. Variation of linear specific deformation (ε) as a function of time, working scenario 2, left limb (LF).

Figure 24 shows the variation diagrams of the specific linear deformation (ε) as a function of time for the three data sets recorded by the strain gauges mounted on the bionic displacement system that equips the right lower limb (RF). Also, the variation diagram of the specific linear average specific deformation (orange line) is drawn.

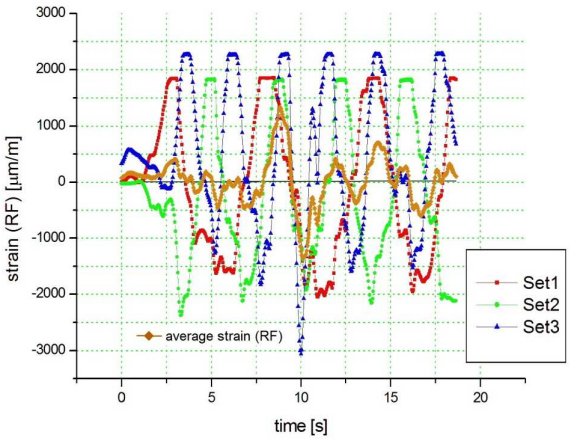

Fig. 24. Variation of specific linear deformation (ε) as a function of time, working scenario 2, right limb (RF).

Figure 25 shows the variation diagrams of the average linear specific deformations (highlighted in Figures 23 and 24) as a function of time.

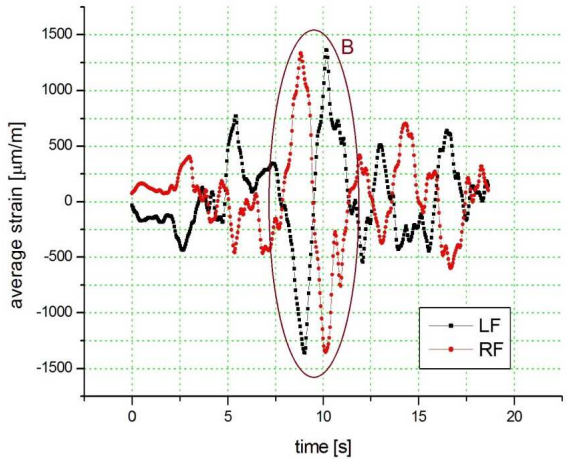

Fig. 25. Variation of mean linear specific deformation (ε_{med}) as a function of time, working scenario 2, left limb (LF), and right limb (RF).

This graphical representation confirms, first, the difficulty of moving with the help of such a bionic system for a person who is experiencing such a device for the first time. Some accommodation with the system can be noticed in the time interval between seconds 7 and 12 (is marked by the circular surface B), the interval for which the present study is relevant. During this time the move was made without the need for additional support. Thus, TTR mounted on the bionic displacement system equipping the lower left limb (LF) indicates a mean linear

specific strain ε_{med} = 2,720.78 μm/m and TTR mounted on the bionic displacement system equipping the right lower limb (RF) indicates a mean linear specific deformation ε_{med} = 2,684.325 μm/m.

Table 1 and Table 2 summarize the results obtained analytically and experimentally. Relative deviations (rel. dev.) are calculated using the following relation:

$$Rel.dev. = \frac{max.val. - min.val.}{max.val.} \cdot 100[\%] \quad (32)$$

Table 1

Experimentally determined normal stresses [σ – S1, σ – S2 (LF), σ – S2 (RF)] and analytical [σ – S1+ rel(14), σ – S2 (LF) + rel(14), σ – S2 (RF) + rel(14)].

σ [MPa] – S1	σ [MPa] – S2 (LF)	σ [MPa] – S2 (RF)
39.807	76.181	75.161
σ [MPa] – S1 +rel(14)	**σ [MPa] – S2 (LF) +rel(14)**	**σ [MPa] – S2 (RF) +rel(14)**
35.794	71.588	71.588
Rel.dev. [%]	**Rel.dev. [%]**	**Rel.dev. [%]**
10.081	6.029	4.753

Table 2

Experimentally determined potential deformation energy [Ud – S1, Ud – S2 (LF), Ud – S2 (RF)] and analytical [Ud – S1+ rel(14), Ud – S2 (LF) + rel(14), Ud – S2 (RF) + rel(14)].

Ud [J] – S1 ($\cdot 10^{-2}$)	Ud [J] – S2 (LF) ($\cdot 10^{-2}$)	Ud [J] – S2 (RF) ($\cdot 10^{-2}$)
1.414	5.181	5.043
Ud [J] – S1 +rel(14) ($\cdot 10^{-2}$)	**Ud [J] – S2 (LF) +rel(14) ($\cdot 10^{-2}$)**	**Ud [J] – S2 (RF) +rel(14) ($\cdot 10^{-2}$)**
1.272	4.869	4.804
Rel.dev. [%]	**Rel.dev. [%]**	**Rel.dev. [%]**
10.042	6.022	4.739

From the perspective of the characteristic diagram normal stress (σ) - specific linear deformation (ε), represented in Figure 26, the potential deformation energy (Ud) for working scenario 1 (S1) represents the surface bounded by points 0ca and for working scenario 2 (S2) represents the area bounded by points 0db.

Because the composite material used does not have a behavior characteristic of ductile materials, the ultimate stress (σ_r) is the reference limit. Thus, the load capacity of the elastic element in S1 is 8% and in S2 is 15%. It is estimated that in dynamic loading mode it can reach 50%. It can be concluded that the cross-section is oversized so that the mass of the bionic displacement system is considerably higher. The study model presented in this paper can be of real use for the optimal sizing of the elastic element.

Of course, the other components can also be reconfigured relatively easily with the help of virtual modeling tools (e.g., the SolidWorks software), according to Figure 27.

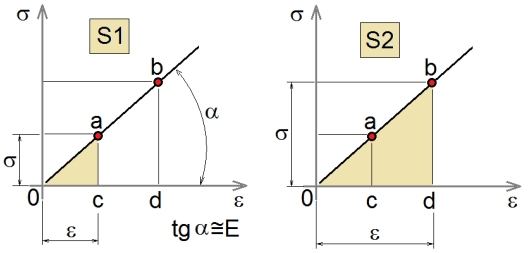

Fig. 26. The characteristic curve σ-ε, in the elastic domain, of the composite material for the two working scenarios, S1 and S2.

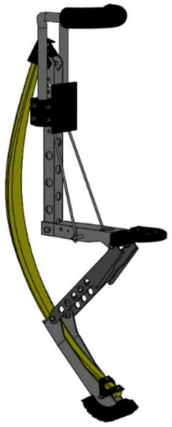

Fig. 27. The bionic displacement system is presented in virtual modeling (SolidWorks software).

4. CONCLUSIONS

In this study, the entire layer (with reference to the elastic element) - laminate, made up of several sheets -, from a macroscopic perspective, is considered homogeneous and anisotropic.

Based on the tests performed, within the limits described by the two working scenarios (S1 and S2) the composite material behaves linear - elastic (reversible deformations are recorded) and in phase with normal stresses σ. For this reason, Hooke's law was adopted as a simplifying calculation hypothesis.

The modeling of the bionic structure in the RDM 7.04 finite element analysis program allowed the evaluation of both the reactions and the efforts, thus identifying the maximum loaded section. The result obtained is validated by the fact that this section is identical to that of the real model. The real model has a variable cross section with a maximum value of the area in the most loaded area.

For this type of application, it was decided to use the electrical strain-gages method which allows the measurement of specific linear deformation ε at frequencies up to 600 Hz using the Spider 8-30 data acquisition system. In this study the selected operating frequency was 25 Hz and Automatic zero balancing. The strain gauge transducers were connected in an adjacent half-bridge circuit.

The evaluation of strains (a total of 2,979 processed data) is performed in two working scenarios: for the case where there is bipedal support (S1) and for the case of unipedal support, for uniform rectilinear movement (S2). In both scenarios, the relative deviations (concerning the potential deformation energy) between the analytically and experimentally obtained results are below 11 percent. This study has relevance especially from the perspective of the possibility to optimally dimension the elastic element so that the bionic displacement system has its mass as small as possible.

5. REFERENCES

[1] Mohamed, A.A., Nader, A.R.M., Bakheet, A., *Low-cost electromechanical bionic model for foot drop gait disability*, ICCIS 2020, IEEE Xplore, doi: 10.1109/ICCIS49240.2020.9257672.

[2] Jianxun, D., Peng, H., Zhiqiang, X., Mabao, L., *Energy absorption of bionic lightweight protective structure with curved tubes under impact loading*, Proceedings o the Institution of Mechanical Engineers, Part L: Journal of Materials: Design and Applications, 2021, doi.org/10.1177/14644207211028254.

[3] Toader, N., Sobek, W., Nickel, K.G., *Energy absorption in functionally graded concrete bioinspired by sea urchin spines*, Journal of Bionic Engineering, 14 (2), 2017, pp.369-378.

[4] Jiafeng, S., Shucai, X., Lihan, X., Jianfei, Z., Meng, Z., *Experimental study on the crashworththiness of bio-inspired aluminum foam-filled tubes under axial compression loading*, Thin-Walled Structures, 155, 2020, doi.org/10.1016/j.tws.2020.106937.

[5] Bhushan, B., *Biomimetics*, Ed. Springer, 2012.

[6] Jabbari, E., *Handbook of Biomimetics and Bioinspiration*, Ed. World Scientific, 2014.

[7] Benyus, J.M., *Biomimicry: Innovation Inspired by Nature*, Perennial, New-York, 2002.

[8] Gregory P. Sutton, Malcolm Burrows, *Biomechanics of jumping of the flea*, The Journal of Experimental Biology 2011.

[9] Cannistraro, J.P. *Elastic Energy and The Kangaroo*, Standford University, 2017.

[10] Morgan, D.L., Proska, U., Warren, D., *Measurements of Muscle Stiffness and the Mechanism of Elastic Storage of Energy in Hopping Kangaroos*, J.Physiol., 282, pp.253-261, 1978.

[11] Kram, R., Dawson, T.J. *Energetic and biomechanics of locomotion by red kangaroos (Macropus rufus*), Comparative Biochemistry and Physiology Part B: Biochemistry and Molecular Biology, 120(1), pp.41-49, 1998.

[12] Biewener, A., Alexander, R.McN, Heglund, N.C., *Elastic energy storage in the hopping of kangoroo rats (Dipodomys spectabilis)*, J.ofZoology, 195, pp.369-383, 1981.

[13] Botean, A.I., *Solutions to improve mobility of the plaster walking boot in patients with pathologies of the lower limb*, Acta Technica Napocensis, Series: Applied Mathematics, Mechanics and Engineering, ISSN 1221-5872, Vol 64(3), pp.415-422, 2021.

[14] Wang, H.W., Zhou, H.W., Gui, L.L., Ji, H.W., Zhang, X.C., *Analysis of effect orientation on Young's modulus for unidirectional fiber reinforced composites*, Composites Part B: Engineering, Volume 56, January 2014, pp.733-739.

[15] Wang, H.W., Zhou, Mishnaevsky, L., Brondsted, P., Wang, L.N., *Single fiber and multifibre unit cell analysis of strength of unidirectional composites*, Comput Mater Sci, 46 (4) (2009), pp.810-820.
[16] Botean, A.I., *Rezistenţa materialelor. Solicitări simple*, Ediţia a-II-a, revizuită şi adăugită, ISBN 978-606-737-407-0, U.T.PRESS, Cluj-Napoca, 2019.
[17] Gurusideswar, S., Srinivasan, N., Velmurugan, R., Gupta, N.K., *Tensile response of epoxy and glass/epoxy composites at low and medium strain rate regimes*, Procedia Engineering, 173, 2017, pp 686-693, doi.org/10.1016/j.proeng.2016.12.148.
[18] Şomotecan, M., *Compozite. Calcul de rezistenţă*, ISBN 973-9471-28-5, U.T.Pres, Cluj-Napoca, 2000.
[19] Gay, D., *Matériaux composites*, 3e édition revue et augmentée, ISBN 2-86601-268-2, Hermès, 1991.
[20] Creţu, A., *Rezistenţa materialelor*, ISBN 973-713-089-8, Editura MEDIAMIRA, Cluj-Napoca, 2005.
[21] Hibbeler, R.C., *Mechanics of Materials*, Sixth Edition, ISBN 0-13-191899-0, Pearson Education International, 2005.
[22] Megson, T.H.G., *Structural and Stress Analysis*, Second Edition, ISBN 978-0-7506-6221-5, Elsevier Butterworth – Heinemann, 2005.
[23] Hoffmann K., *An Introduction to Measurements using Strain Gages*, Publisher Hottinger Baldwin Messtechnik GmbH, Darmstadt, 1989.
[24] Hoffmann K., *An introduction to stress analysis and transducer design using strain gauges*, HBM test, and measurement, 2012.
[25] Kobayashi A.S., *Handbook on Experimental Mechanics*, Second Revised Edition, Publisher Society for Experimental Mechanics, 1993.
[26] Sciammarella C.A., Sciammarella F.M., *Experimental Mechanics of Solids*, Publisher John Wiley & Sons, Ltd, 2012.
[27] Stein P.K., *Strain gauge history and the end of the twentieth century*, Exp. Techn., pp.15-16, 2001.
[28] TecQuipment, *SM1009 Strain gauge trainer*. User guide, 2011.
[29] Venkathesan S.P., *Mechanical measurements*. 2nd edition, John Wiley & Sons Ltd, 2015.
[30] Webster J.G., *The measurement, instrumentation, and sensors*, CRC Press LLC, 1999.

Evaluarea energiei potenţiale de deformare din elementul elastic al unui sistem bionic de deplasare

Rezumat. În această lucrare, prezint o abordare multidisciplinară pentru identificarea secțiunii transversale maxim solicitată a elementului elastic al sistemului bionic de deplasare (a cărui concepție trebuie să se bazeze pe principiul biomimetismului), precum și evaluarea stării de tensiuni și deformaţii, respectiv a energiei potenţiale de deformare acumulate. Acest studiu implică modelarea structurii prin intermediul metodei elementelor finite pentru evaluarea eforturilor (forța axială N, forța tăietoare T și momentul încovoietor Mi), utilizarea relaţiilor analitice pentru calcularea tensiunilor mecanice și a energiei potențiale de deformare precum și metoda tensometriei electrice rezistive pentru evaluarea experimentală a deformaţiilor specifice liniare. Evaluarea deformaţiilor (un total de 2.979 de date prelucrate) se realizează în doua scenarii de lucru: pentru cazul în care există sprijin bipodal (S1) şi pentru cazul sprijinului unipodal, pentru mișcarea rectilinie uniformă (S2). În ambele scenarii, abaterile relative (privind energia potențială de deformare) între rezultatele obținute analitic și experimental sunt sub 11%. Acest studiu are relevanță, mai ales din perspectiva posibilității dimensionării optime a elementului elastic astfel încât sistemul bionic de deplasare să aibă masă proprie cât mai redusă.

Adrian Ioan BOTEAN, Lecturer, Ph.D.Eng., Technical University of Cluj-Napoca, Department of Mechanical Engineering, 103-105 Muncii Blvd., 400641, Cluj-Napoca, +40–264–401751, Adrian.Ioan.Botean@rezi.utcluj.ro.